

EyeAgent: An Agentic AI System for Multimodal Clinical Decision Support in Ophthalmology

Author:

Danli Shi, MD^{1,2#}, Xiaolan Chen, MD^{1#}, Bingjie Yan, MSc^{1#}, Weiyi Zhang, MSc¹, Pusheng Xu, MD¹, Jiancheng Yang, PhD³, Ruoyu Chen, MD¹, Siyu Huang, DEng⁴, Bowen Liu, MSc¹, Xinyuan Wu, MD¹, Meng Xie, MD¹, Ziyu Gao, MEng¹, Yue Wu, MD¹, Senlin Lin, MSc⁵, Kai Jin, MD⁶, Xia Gong, MD¹, Yih Chung Tham, PhD⁷, Xiujuan Zhang, PhD⁸, Li Dong, MD⁹, Yuzhou Zhang, PhD¹⁰, Jason Yam, PhD¹⁰, Guangming Jin, PhD¹¹, Xiaohu Ding, MD¹¹, Haidong Zou, MD⁵, Yalin Zheng, PhD¹², Zongyuan Ge, PhD¹³, Mingguang He, MD^{1,2,14*}

Affiliations:

1. School of Optometry, The Hong Kong Polytechnic University, Hong Kong.
2. Research Centre for SHARP Vision (RCSV), The Hong Kong Polytechnic University, Hong Kong.
3. Swiss Federal Institute of Technology Lausanne (EPFL), Lausanne, Switzerland.
4. School of Computing, Clemson University, Clemson, SC, USA.
5. Shanghai Eye Diseases Prevention & Treatment Center/ Shanghai Eye Hospital, School of Medicine, Tongji University, Shanghai, China.
6. Department of Ophthalmology, The Second Affiliated Hospital, School of Medicine, Zhejiang University, Hangzhou, China.
7. Centre for Innovation and Precision Eye Health & Department of Ophthalmology, Yong Loo Lin School of Medicine, National University of Singapore, Singapore.
8. Department of Ophthalmology, The University of Hong Kong, Hong Kong.
9. Beijing Tongren Eye Center, Beijing key Laboratory of Intraocular Tumor Diagnosis and Treatment, Beijing Ophthalmology & Visual Sciences Key Laboratory, Medical Artificial Intelligence Research and Verification Key Laboratory of the Ministry of Industry and Information Technology, Beijing Key Laboratory of Intelligent Diagnosis, Treatment and Prevention of Blinding Eye Diseases, Beijing Tongren Hospital, Capital Medical University, Beijing, China.
10. Department of Ophthalmology and Visual Sciences, The Chinese University of Hong Kong, Hong Kong.
11. State Key Laboratory of Ophthalmology, Zhongshan Ophthalmic Center, Sun Yat-sen University, Guangdong Provincial Key Laboratory of Ophthalmology and Visual Science, Guangdong Provincial Clinical Research Center for Ocular Diseases, Guangzhou, China.
12. Department of Eye and Vision Science, University of Liverpool, Liverpool, UK.
13. AIM for Health Lab, Faculty of Information Technology, Monash University, Melbourne, Victoria, Australia.

14. Centre for Eye and Vision Research (CEVR), 17W Hong Kong Science Park, Hong Kong.

Danli Shi, Xiaolan Chen, Bingjie Yan contributed equally to this article.

Correspondence

*Danli Shi, School of Optometry, The Hong Kong Polytechnic University, Hong Kong, China. Email: danli.shi@polyu.edu.hk.

*Mingguang He, Department of Experimental Ophthalmology, The Hong Kong Polytechnic University, Hong Kong, China. Email: mingguang.he@polyu.edu.hk

Abstract

Artificial intelligence has shown promise in medical imaging, yet most existing systems lack flexibility, interpretability, and adaptability—challenges especially pronounced in ophthalmology, where diverse imaging modalities are essential. We present EyeAgent, the first agentic AI framework for comprehensive and interpretable clinical decision support in ophthalmology. Using a large language model (DeepSeek-V3) as its central reasoning engine, EyeAgent interprets user queries and dynamically orchestrates 53 validated ophthalmic tools across 23 imaging modalities for diverse tasks including classification, segmentation, detection, image/report generation, and quantitative analysis. Stepwise ablation analysis demonstrated a progressive improvement in diagnostic accuracy, rising from a baseline of 69.71% (using only 5 general tools) to 80.79% when the full suite of 53 specialized tools was integrated. In an expert rating study on 200 real-world clinical cases, EyeAgent achieved 93.7% tool selection accuracy and received expert ratings of $\geq 88\%$ across accuracy, completeness, safety, reasoning, and interpretability. In human-AI collaboration, EyeAgent matched or exceeded the performance of senior ophthalmologists and, when used as an assistant, improved overall diagnostic accuracy by 18.51% and report quality scores by 19%, with the greatest benefit observed among junior ophthalmologists. These findings establish EyeAgent as a scalable and trustworthy AI framework for ophthalmology and provide a blueprint for modular, multimodal, and clinically aligned next-generation AI systems.

Keywords: medical AI agent, large language model, ophthalmology, tool integration, clinical decision support, trustworthy AI

Introduction

Artificial intelligence (AI) has made significant progress in medical research, with large language models (LLMs) and vision-language models showing particular promise.¹⁻³ In ophthalmology, AI has been applied to a wide spectrum of tasks, including screening for vision-threatening diseases,⁴ segmenting ocular structure,⁵ generating medical reports and interactive question answering.⁶ However, these systems fall short of true clinical intelligence: they cannot emulate the reasoning of a clinician, flexibly handle complex and heterogeneous tasks, or provide transparent, evidence-based justifications. Moreover, they lack the autonomy and adaptability necessary for seamless integration into real-world clinical workflows.

Ophthalmology is a unique challenge for intelligent systems. Patient evaluation often requires integration of multiple imaging modalities including color fundus photography (CFP), optical coherence tomography (OCT), fundus fluorescein angiography (FFA), and indocyanine green angiography (ICGA)—each offering distinct structural or functional insights.^{7,8} Clinical reasoning involves iterative hypothesis testing, longitudinal data synthesis, and interdisciplinary input. In difficult cases, uncertainty may be resolved only through additional investigations or dynamic follow-up planning. Such context-rich and sequential workflows call for AI systems capable of multimodal integration, domain-specific reasoning, and adaptive decision-making.

Recent multimodal foundation models offer early progress but remain hampered by critical limitations. End-to-end architectures often operate as “black boxes,” undermining interpretability and trust.⁹ LLMs, especially, are prone to hallucination, raising safety concerns in clinical deployment.^{9,10} Training large models further demands extensive annotated datasets that are scarce due to privacy and proprietary constraints.¹¹ Furthermore, most approaches prioritize retraining monolithic models rather than leveraging validated task-specific AI tools or integrating domain knowledge from guidelines and textbooks, leading to redundant computation, poor transferability, and limited clinical relevance.

Agentic AI systems present a promising road.^{12,13} These systems can autonomously interpret instructions, retrieve relevant knowledge, and orchestrate external tools to accomplish complex, multi-step tasks.¹⁴ Compared to end-to-end models, agentic approaches provide (i) interpretability, as each reasoning step is evidence-based and traceable; (ii) reduced hallucination, by grounding outputs in verified tools and databases; and (iii) modularity and scalability, as new capabilities can be integrated without retraining entire models. Such frameworks have demonstrated utility in molecular biology¹⁵, genomics¹⁶ and drug discovery¹⁷, particularly where reasoning across heterogeneous inputs is required.

Here we introduce EyeAgent, the first agentic AI system for multimodal ophthalmic analysis. EyeAgent uses an LLM (DeepSeek-V3) as its central reasoning core, dynamically orchestrating 53 validated

ophthalmic tools spanning 23 modalities (**Fig. 1a**). These tools support classification, segmentation, modality translation, 3D reconstruction, biomarker extraction, and free-text interpretation (**Fig. 1d**). To ensure domain-specific grounding, EyeAgent incorporates retrieval-augmented generation (RAG) from 14 authoritative ophthalmology textbooks (see Table S1 of the Supplementary Appendix). Operated through a natural language interface, it enables interactive task definition and execution of dynamic reasoning pipelines encompassing planning, tool selection, result synthesis, and output generation for both clinical decision support and medical education (**Fig. 1b**).

We comprehensively evaluated EyeAgent at both module and system levels using diverse internal and external datasets comprising 862490 samples, including static images and longitudinal clinical cases (**Fig. 1c**). At the module level, we benchmarked performance in classification, segmentation, and report generation. At the system level, we conducted four evaluations: (i) ablation study to quantify tool contributions; (ii) head-to-head comparisons with GPT-4o and human experts to assess versatility and robustness; (iii) external validation on 200 real-world cases, with board-certified ophthalmologists rating performance across six dimensions—tool-use accuracy, completeness, safety, reasoning, and interpretability; and (iv) a multi-center human–AI reader study involving 27 ophthalmologists from 11 centers, stratified into senior (≥ 5 years of experience) and junior groups, to evaluate EyeAgent’s ability to support clinical workflows.

Figure 1. Overview of EyeAgent system and study design.

a, Core architecture of EyeAgent, which integrates a large language model with 53 specialized ophthalmic tools and a domain-specific knowledge base. The system supports 6 task types, 23 data modalities, and 260 ophthalmic conditions.

b, EyeAgent is designed to address complex clinical scenarios, including hierarchical decision support, quantitative image analysis, medical education, decision conflict resolution, and cross-specialty longitudinal analysis.

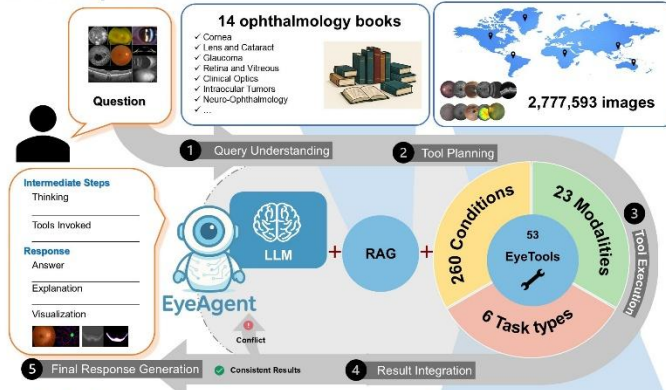
c. Evaluation pipeline spanning five parts: tool-level validation, module-level ablation, case comparison analysis, expert rating study and human-AI reader study.

d, Landscape of integrated EyeTools categorized by function and modality.

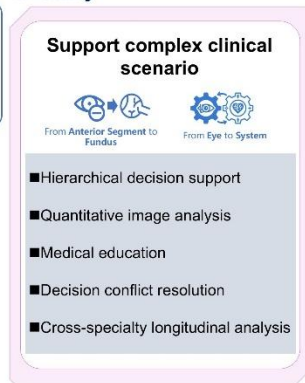
Abbreviations: LLM, large language model; CFP, color fundus photography; FFA, fundus fluorescein angiography; OCT, optical coherence tomography; ICGA, indocyanine green angiography; SLO, scanning laser ophthalmoscopy; MRI, magnetic resonance imaging; FAF, fundus autofluorescence; DR,

diabetic retinopathy; AMD, age-related macular degeneration; RVO, retinal vein occlusion; PM, pathological myopia; CNV, choroidal neovascularization; RD, retinal detachment; MH, macular hole; CSC, central serous chorioretinopathy; CME, cystoid macular edema; CVD, cardiovascular disease.

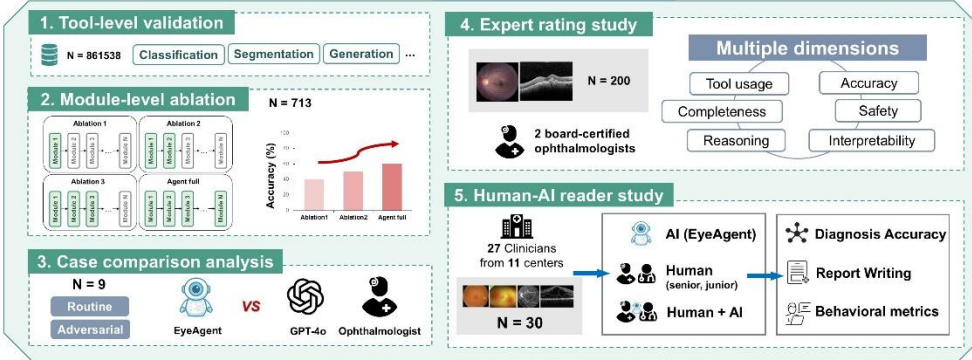
a. Development



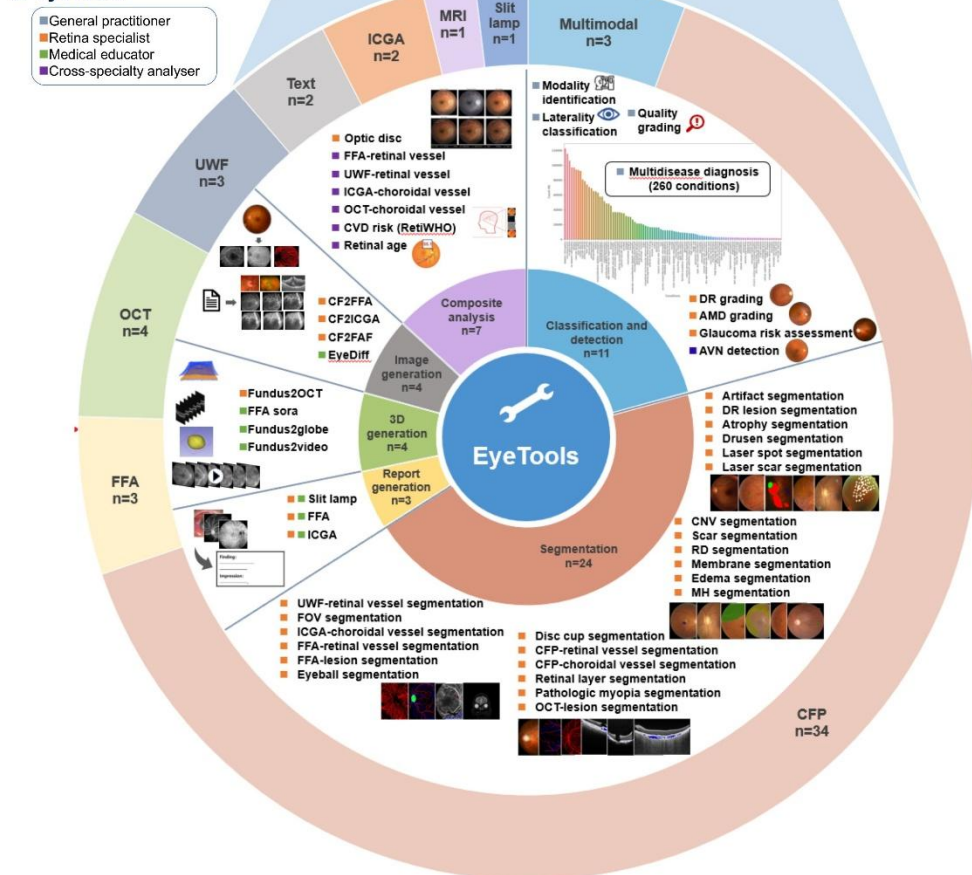
b. Utility



c. Evaluation



d. EyeTools



Methods

EYEAGENT SYSTEM ARCHITECTURE

EyeAgent is an agentic system designed to manage multimodal ophthalmic tasks through domain-specific tool integration and autonomous reasoning. The system comprises two main components (**Fig. 1**): (1) agent core, powered by DeepSeek-V3, responsible for reasoning, planning, and tool orchestration; and (2) curated tool suite (EyeTools), a collection of domain-optimized AI models covering diverse ophthalmic tasks. The agent core and EyeTools are integrated via LangChain (<https://langchain.com/>, accessed 15 June 2025). Tool inputs and outputs are verified with Pydantic (<https://github.com/pydantic/pydantic>, accessed 15 June 2025) to ensure schema compliance. The reasoning workflow follows five stages: (i) query interpretation, (ii) tool planning, (iii) execution, (iv) result integration, and (v) response generation. EyeAgent supports free-text queries and 23 ophthalmic image modalities. Upon receiving a case, the agent interprets user intent, generates a tool-use plan, monitors intermediate outputs, and revises steps if inconsistencies are detected. Outputs include not only diagnostic results but also explanations and visualizations, ensuring clinical transparency and adaptability across diverse tasks.

INTEGRATION OF EYEAGENT AND EYETOOLS

EyeTools is the most functionally comprehensive module of EyeAgent, comprising 53 models derived from prior work and newly optimized for clinical workflows. These cover 260 eye diseases and 23 imaging modalities, including CFP, OCT, FFA, ICGA, and clinical texts.

Classification tools return both the most likely label and alternative predictions above defined thresholds. Visual outputs (e.g., segmentations) undergo post-processing for interpretability: lesion counts, areas, and severity metrics are extracted, and synthetic images may be re-analyzed for cross-modality validation. All tools follow a structured input-output format with defined usage conditions and can operate independently or in combination under a unified planning module. A complete list of tools is provided in Table S2 of the Supplementary Appendix.

Based on their clinical functions within the workflow, the 53 tools are grouped into four categories: general practitioner, retina specialist, medical educator, and cross-specialty analyser:

General practitioner - basic tasks such as modality recognition (23 image types), image quality assessment, laterality classification, and broad disease screening (260 conditions).

Retina specialist - subspecialty-level diagnosis, subtyping, and anatomical quantification. Supported tasks include diabetic retinopathy (DR) detection, age-related macular degeneration (AMD) staging, glaucoma

risk assessment, and pathological myopia classification (MetaPM).^{18,19} Specialist segmentation tools provide information of anatomical structures and lesions. For example, in CFP images, the model segments microaneurysms, hemorrhages, hard exudates, and retinal vessels to enable quick lesion localization and quantification. In OCT analysis, it identifies all the retinal layers and detects pathological features like macular edema and retinal tears. In FFA images, the system segments neovascularization, leakage regions, and non-perfusion areas,²⁰ aiding assessment of CNV and other vascular disorders. Image generation models can synthesize images like FFA from CFP to aid further clinical interpretation when conflicting outputs arise between the above specialist tools.²¹⁻²³ Quantitative analysis tools compute clinically relevant metrics, including optic disc and cup measurements for glaucoma risk assessment and choroidal vascularity indices for monitoring pathological myopia, contributing to explainable, metric-driven care.²⁴⁻²⁸

Medical educator - incorporates generative models to support education and communication. Text generation models produce structured reports with diagnostic impressions and follow-up recommendations.^{6,29,30} Text-to-image generation models synthesize disease-specific images with characteristic findings,³¹ while 3D generation enables intuitive visualization of complex anatomical or pathological features, facilitating education for both clinicians and patients.³²⁻³⁵

Cross-specialty analyzer - extends ophthalmic imaging into systemic health domains. Retinal vessel analysis models compute hundreds of parameters, such as vessel density, arteriole-to-venule ratio, tortuosity, and branching angle.^{26,36,37} Detection of arteriovenous nicking aids hypertensive retinopathy assessment, while regression models predict cardiovascular risk and retinal age directly from fundus photographs.²⁸ These tools broaden the role of ophthalmic imaging, enabling systemic disease screening and longitudinal health monitoring.

Knowledge base - RAG enhances EyeAgent's reasoning by grounding outputs in authoritative ophthalmology literature.³⁸ Linking responses to curated references improves reliability for differential diagnosis, image interpretation, and treatment guidance.

SCENARIO-BASED WORKFLOWS

To test EyeAgent in clinically realistic contexts, we designed five representative workflows reflecting common diagnostic and decision-making challenges: (1) hierarchical decision support, (2) quantitative image analysis, (3) medical education, (4) decision conflict resolution, and (5) cross-specialty longitudinal analysis. Each workflow involved multimodal inputs (e.g., CFP, OCT, text) and tool orchestration via LLM-based planning, simulating real-world physician behavior from initial screening to patient communication.

PERFORMANCE EVALUATION OF EYEAGENT

Tool-level assessment

Tool-level validation was performed on public and in-house datasets comprising 861,538 ophthalmic images (796,233 classification; 65,305 segmentation). Details are in Table S3 of the Supplementary Appendix. Classification tools were evaluated using area under the receiver operating characteristic curve (AUC), accuracy, sensitivity, specificity, and F1 score. Segmentation was evaluated by Dice similarity coefficient and intersection-over-union (IoU).

Ablation and benchmarking

To evaluate the contribution of different tool categories in EyeAgent, we defined five progressive configurations: Ablation 1 (Base, 5 general tools): modality-label classification covering image quality, laterality, image modality, and 260 diseases conditions, establishing baseline performance. Ablation 2 (Extended, 14 tools): Adds disease-specific classifiers targeting common ophthalmic conditions (e.g., diabetic retinopathy, AMD, glaucoma, pathological myopia) to improve diagnostic specificity. Ablation 3 (Enhanced, 35 tools): Incorporates multi-modal anatomical and pathological segmentation, enabling fine-grained localization of lesions, retinal layers, and vasculature across CFP, OCT, FFA, ICGA, and UWF images. Ablation 4 (Generative, 46 tools): Introduces cross-modality generation and automated reporting, including fundus-to-FFA/OCT synthesis and modality-specific structured report generation, supporting multimodal reasoning. (5) Ablation 5 (Comprehensive, 53 tools): Complete toolset with quantitative vascular analysis, demographic estimation, and retrieval-augmented generation (RAG) for contextualized diagnostic assistance.

For CFP evaluation, we used ODIR5K³⁹, APTOS 2019⁴⁰, DeepDRiD⁴¹, HPMI⁴², and RFMiD⁴³, comprising 451 images across 13 diagnostic categories (normal; multiple DR stages; pathological myopia subtypes; retinal vein occlusion; central serous chorioretinopathy; retinal detachment; epiretinal membrane; glaucoma).

For OCT evaluation, we used OCTID⁴⁴ and OCTDL⁴⁵, comprising 262 images across 8 categories (normal; wet AMD; dry AMD; diabetic macular edema; epiretinal membrane; macular hole; retinal vein occlusion; central serous chorioretinopathy). Disease distributions for CFP and OCT are shown in Figure S3 of the Supplementary Appendix.

For all configurations, EyeAgent outputs were benchmarked against expert-annotated ground truth. Accuracy was defined as exact diagnostic agreement, with grading or subtype discrepancies counted as incorrect.

Case comparison against GPT-4o and human physicians

We conducted a head-to-head comparison on 9 curated cases spanning multiple modalities and tasks (diagnosis, quantification, education, biomarker analysis, adversarial inputs). Three groups were compared: EyeAgent (tool-augmented reasoning), GPT-4o (direct responses without external tools), and a board-certified ophthalmologist (>5 years' experience, unaided). To ensure comparability, responses were capped at 100 words. Outputs were qualitatively assessed for accuracy, reasoning transparency, and robustness. Cases were chosen to represent a spectrum of difficulty, ambiguity, and susceptibility to hallucination.

Expert rating study

To quantitatively evaluate EyeAgent in simulated clinical workflows, we assessed 200 ophthalmic cases covering CFP and OCT modalities and 12 common conditions, including DR, AMD, and pathological myopia (data distribution in Table S4 of the Supplementary Appendix). For each case, EyeAgent generated a transparent diagnostic output comprising intermediate results (reasoning steps, invoked tools) and a final report detailing modality, image quality, laterality, diagnosis, evidence, and recommendations (prompts and example cases in Table S5 and Figure S4 and of the Supplementary Appendix).

Two board-certified ophthalmologists (>5 years' experience) independently rated outputs on five dimensions—accuracy, completeness, safety, reasoning, and interpretability—using a 3-point scale (1 = poor, 2 = acceptable, 3 = good; maximum total score 15; criteria in Table S6 of the Supplementary Appendix). Discrepancies were resolved by adopting the lower score. Tool usage accuracy was evaluated against ophthalmologist-defined ground truth, with metrics defined as: correct tool (matched ground truth), incorrect tool (missed ground truth), and tool not in ground truth (additional tool invoked). Accuracy was calculated as the proportion of ground truth tools correctly selected, excluding tools not in the ground truth.

Multi-center human-AI collaboration study

A reader study was conducted online via the Qualtrics platform from July 3 to August 3, 2025, involving 27 ophthalmologists from 11 centers in mainland China and HKSAR (9 senior [≥ 5 years], 18 junior [< 5 years]). No restrictions were applied to subspecialty. Readers first assessed each case unaided, providing free-text diagnoses and structured reports including supporting evidence and management recommendations. Diagnostic confidence was rated on a 5-point Likert scale (1 = not confident at all; 5 = highly confident). After submitting initial assessments, readers were shown EyeAgent's outputs and allowed to revise their diagnoses and reports, followed by re-rating confidence. Readers also indicated the

extent of adoption of EyeAgent’s outputs (0%, 25%, 50%, 75%, 100%) and the specific components adopted (e.g., image details, diagnosis, management).

A reference set comprising ground truth diagnoses and a checklist-based scoring rubric for clinical reports was developed by two experienced ophthalmologists. The rubric included 197 items covering key observations, diagnostic reasoning, and management decisions, based on expert consensus and authoritative guidelines. Each item was scored as 1 (present) or 0 (absent), and normalized completeness scores were calculated per report.

Diagnostic outputs from readers and EyeAgent were compared to ground truth using GPT-4o, prompted to classify responses as correct, partially correct, or incorrect. Proportions for each category were calculated across reader groups and model outputs (prompt template in Table S7 of the Supplementary Appendix). All AI- and human-generated responses were subsequently reviewed by an experienced ophthalmologist for quality assurance. Agreement between GPT-4o and expert ratings was quantified using Cohen’s kappa. For report completeness, two expert graders independently scored each report using the 197-item checklist; final scores were averaged and normalized to a 0–1 scale. Inter-rater reliability was assessed using the intraclass correlation coefficient (ICC).

STATISTICAL ANALYSIS

Descriptive statistics were used to summarize all performance metrics. In the expert rating study, subgroup comparisons were performed using the Mann-Whitney test. For the reader study, statistical tests were selected based on data type and distribution: Wilcoxon rank-sum test, Wilcoxon signed-rank test, Fisher’s exact test, or McNemar–Bowker test, with Holm correction applied for multiple comparisons. 95% confidence intervals were calculated using the Wilson method. Inter-rater reliability was assessed using Cohen’s kappa or ICC, as appropriate. All analyses were conducted in R (v4.3.0) using two-sided tests, with a significant level of $P < 0.05$.

Results

EYEAGENT SYSTEM OVERVIEW AND CLINICAL WORKFLOW SIMULATION

To bridge the gap between specialized ophthalmic AI models and real-world clinical workflows, we developed EyeAgent, an agentic system that orchestrates 53 validated tools (EyeTools, see the Table S2 of the Supplementary Appendix) across diverse scenarios. These tools, refined from our prior research, are

organized into five categories: classification and detection, segmentation and quantification, regression, generation, and RAG.

Classification and detection tools span general screening tasks (e.g., modality and laterality recognition, image quality assessment, and pre-screening across 260 ophthalmic conditions) as well as specialist diagnostic models for DR, AMD, glaucoma, and pathological myopia. These models serve as clinical gatekeepers for triage and referral, with screening AUCs > 0.823 (see the Table S8 of the Supplementary Appendix) and specialist models validated in prior publications.⁴⁶⁻⁴⁸

Segmentation and quantification tools provide automated annotation of anatomical structures and pathological lesions, producing quantitative metrics such as optic disc parameters, retinal and choroidal vascular indices, lesion counts, and lesional areas. These objective outputs enhance interpretability and downstream decision-making (see Figure S1 and Table S9 of the Supplementary Appendix, and prior publications).^{20,24,26,27}

Regression models extend beyond ocular disease, predicting clinically relevant traits such as retinal age and WHO cardiovascular risk scores,²⁸ thereby linking ophthalmic imaging to systemic health screening.

Generation tools span text (e.g., structured report generation, modality-specific summarization),^{6,29,30} 2D image synthesis (e.g., cross-modality generation),^{21-23,31,33} 3D generation and reconstruction (e.g., synthetic FFA videos⁴⁹, eyeball reconstruction for high myopia^{34,35}), facilitating documentation, communication, and patient education.

Finally, RAG modules draw on 14 ophthalmology textbooks to provide evidence-based explanations and mitigate hallucination risks, validated previously in EyeGPT.³⁸

Using EyeTools, EyeAgent autonomously executes clinician-like workflows in five representative scenarios (**Fig. 2**). In hierarchical decision support, EyeAgent simulates real-world triage and referral chains, starting from general eye care practitioners to expert-level diagnosis, with confidence scores and visual outputs to support clinical decisions. In quantitative image analysis, it segments anatomical and pathological features to get lesion maps and multidimensional metrics (e.g., area, count, thickness), enabling precise staging, planning, and monitoring. In medical education, it enables interactive learning through multimodal visualization (e.g., abstract concept demonstration through 3D anatomical reconstructions), cross-modality comparisons, and textbook-grounded explanations. In decision conflict resolution, it reconciles discordant findings across tools, invoking advanced tools for secondary analysis or multimodal image generation to augment information. In cross-specialty longitudinal analysis, it integrates ocular biomarkers to reflect systemic health, such as estimating cardiovascular risk from retinal images, to

support early detection and inter-specialty communication. Collectively, these workflows demonstrate how EyeAgent unifies isolated AI functions into comprehensive, interpretable, and adaptive clinical support.

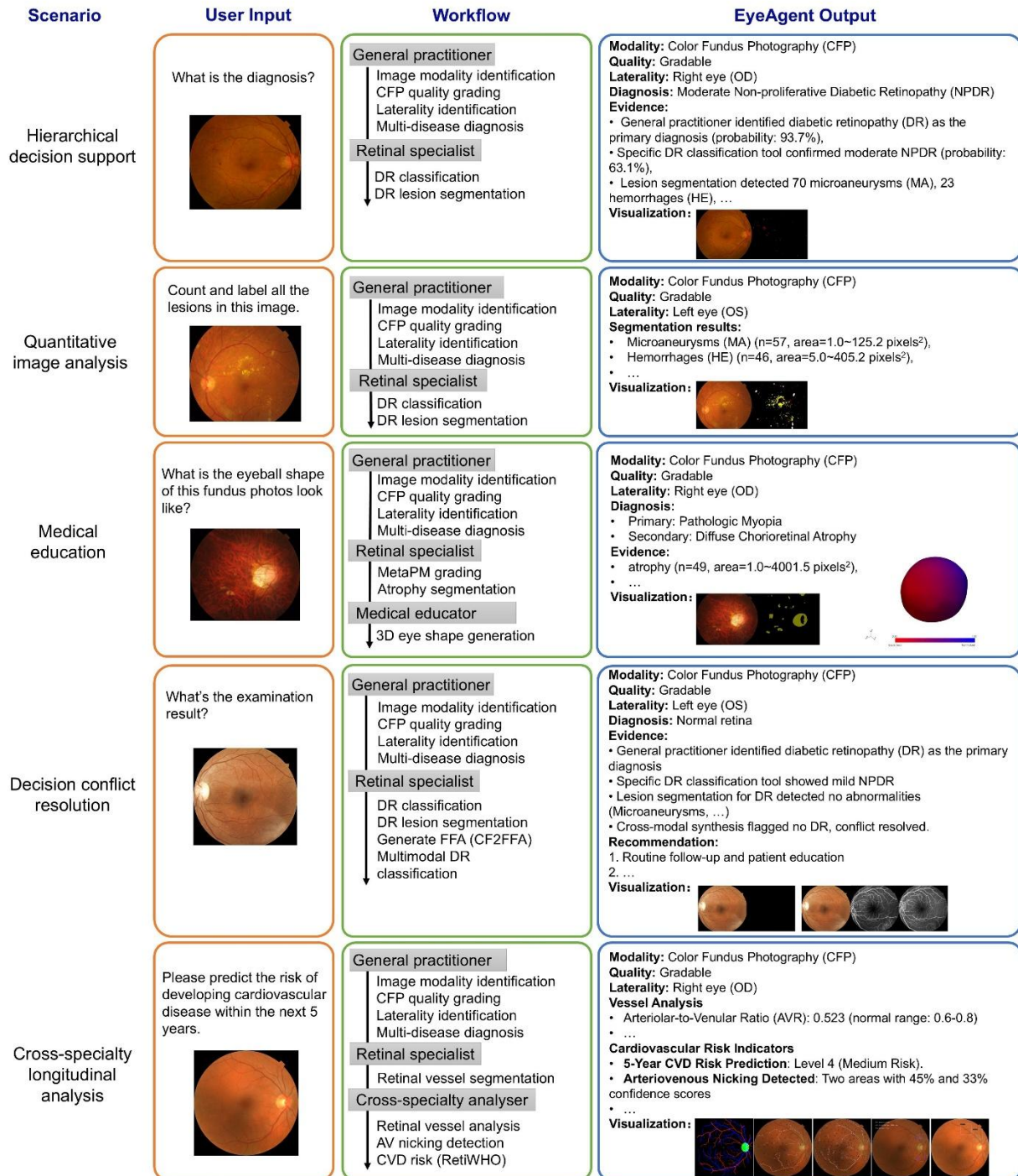


Figure 2. Representative clinical workflows enabled by EyeAgent. Five real-world ophthalmic workflows supported by EyeAgent through dynamic tool orchestration and reasoning: (1) hierarchical decision support: from general screening to specialist-level disease subtyping and risk stratification; (2)

quantitative image analysis: lesion segmentation and measurement for staging and monitoring; (3) medical education: visualization of anatomy, cross-modality comparisons, and textbook-based explanations; (4) decision conflict resolution: addressing inconsistencies across tools or modalities through multi-level analysis; (5) cross-specialty longitudinal analysis: systemic risk prediction based on ocular biomarkers.

Abbreviation: CFP, color fundus photography; DR, diabetic retinopathy; PM, pathological myopia; CNV, choroidal neovascularization; FFA, fundus fluorescein angiography; AVR, arteriovenous ratio.

MODULE-LEVEL ABLATION AND PERFORMANCE BENCHMARK

To objectively evaluate whether each tool category was indispensable and whether the system design was optimal, we performed stepwise ablation and benchmarking. Five configurations were tested, gradually expanding the toolset (see Table S10 of the Supplementary Appendix).

Across 451 CFP images (13 diagnostic categories) and 262 OCT images (8 categories), overall diagnostic accuracy improved from 69.71% in the Base configuration (5 general tools) to 80.79% in the Comprehensive configuration.

The largest gain occurred from Base to Extended (+9.11% overall; +16.42% OCT), primarily due to disease-specific diagnostic modules. Adding segmentation tools in the Enhanced configuration yielded a further +1.68% gain, enabling finer lesion localization and structural analysis, particularly in OCT (+2.67%).

Generative capabilities, including cross-modality synthesis and automated reporting, produced marginal improvement for CFP (+0.45%) but a slight OCT decrease (-0.38%), likely due to increased reasoning complexity. The final comprehensive configuration, incorporating RAG and quantitative vascular analysis, achieved a small additional gain (+0.14% overall), suggesting that these tools primarily enhance contextual reasoning rather than raw classification performance.

Overall, 82% of the performance gains were achieved by adding disease-specific classification and segmentation tools, highlighting their dominant role in boosting accuracy.

COMPARISON WITH GPT-4O AND HUMAN

To demonstrate versatility and robustness, we compared EyeAgent's output with GPT-4o and human ophthalmologists across 9 representative clinical scenarios (7 routine, 2 adversarial; **Fig. 3**). These cases were designed to evaluate the benefits of tool-grounded reasoning in mitigating hallucinations and enhancing clinical reliability.

EyeAgent demonstrated advantages in structured reasoning, image grounding, and adaptive workflow execution. In hierarchical decision-making, GPT-4o identified the correct disease but misclassified modality and laterality, whereas EyeAgent achieved complete task alignment, producing triage outputs with confidence scores and lesion visualizations comparable to human experts. In quantitative analysis, human ophthalmologists described lesions verbally, and GPT-4o produced only text-based summaries. By contrast, EyeAgent generated lesion maps and quantitative measurements, enabling precise description. For education tasks, GPT-4o frequently omitted critical findings (e.g., neovascularization) or produced distorted visuals. EyeAgent provided structured, visually coherent responses using segmentation maps, synthetic angiography, and anatomically aligned 3D generation, delivering concrete visual explanations that augmented human teaching. In systemic risk prediction, GPT-4o identified relevant biomarkers but lacked quantification. EyeAgent computed vascular parameters (CRAE, CRVE, AVR) to provide accurate risk stratification.

In adversarial cases, GPT-4o was misled by artifacts or misleading prompts, whereas EyeAgent correctly recognized artifacts through segmentation and resolved uncertainty via multi-tool verification.

Together, these findings highlight that tool-augmented reasoning enables EyeAgent to deliver more accurate, interpretable, and clinically grounded outputs than general-purpose LLMs. While clinicians contribute contextual judgment and safety, EyeAgent adds quantification and visualization, underscoring their complementary potential in clinical workflows.

a. Routine cases

Task	User Input	Human Answer	GPT-4o	EyeAgent
Hierarchical diagnosis (CRVO, UWF-SLO)	What is the potential diagnosis? (provide me the modality, laterality and diagnosis) 	Modality: Ultra-wide field Scanning Laser Ophthalmoscopy Laterality: Left eye (OS) Diagnosis: Central retinal vein occlusion	Modality: Color fundus photography Laterality: Right eye Diagnosis: Central retinal vein occlusion (CRVO) — evidenced by dilated tortuous veins, flame-shaped hemorrhages, and optic disc swelling.	Modality: Scanning laser ophthalmoscopy (probability: 98.8%) and Ultra-wide field imaging (91.2%) Laterality: Left eye (OS, 87.1%) Diagnosis: Retinal vein occlusion (93.6%), central retinal vein occlusion (87.8%)
Visual explainable diagnosis (MH, OCT)	Is there any abnormality? provide me the diagnosis and label the lesions 	OCT of the macula shows a full-thickness macular hole and intra-retinal cyst.	The OCT image shows a full-thickness macular hole (FTMH), characterized by a complete retinal defect at the fovea. The edges of the hole are elevated, with adjacent cystoid spaces indicating intraretinal edema. A possible posterior vitreous separation is also visible. 	This OCT (Optical Coherence Tomography) image of right eye (OD) demonstrates Macular Hole (MH, Top 1 predicted condition) and further validated by segmentation. Segmentation detected macular hole lesion (n=1, area=19,828.0 pixels ²) and retinal fluid lesion (n=12, areas=1.0-572.5), which may indicate associated retinal edema or other fluid-related pathologies:
Quantitative lesion counting (AMD, CFP)	Count, label, and measure the diameter of all the drusen in the image. 	CFP shows diffuse retinal drusen.	In this fundus image, a total of 97 drusen were detected and labeled. The diameters of the drusen ranged from approximately 24.6 μm to 132.4 μm . Each drusen is marked and numbered in the annotated image. 	The image shows 816 drusen in the left eye (OS), with diameters ranging from very small to large (0.1 - 358.2 μm). The mean diameter is approximately $\sim 120.8 \mu\text{m}$. The presence of drusen, especially larger ones, may indicate early to intermediate age-related macular degeneration (AMD) . Segmentation maps are available for review:
Report generation with lesion grounding (Laser spots, FFA)	Can you create a medical assessment report from this image and label the lesions? 	Modality: Fundus Fluorescein Angiography (FFA) Laterality: OD Findings: FFA shows retinal neovascularization with dye leakage, widespread hyperfluorescent microaneurysms across the retina, and laser spots in the peripheral retina. Impression: proliferative diabetic retinopathy, post-photocoagulation	Modality: Fluorescein Angiography (FA) Laterality: Presumed Right Eye Findings: Punctate hyperfluorescent foci are visible in the superior retina, consistent with retinal pigment epithelium (RPE) mottling. A focal hyperfluorescent leakage point is present inferotemporal to the fovea. The macula shows a preserved foveal avascular zone without significant ischemia. Impression: Chronic RPE alterations with focal leakage suggestive of microaneurysm or macular telangiectasia. No evidence of neovascularization or vasculitis. Further evaluation may be warranted to assess for chronic inflammatory or vascular pathology. 	Medical Report: Fluorescein Angiography (FFA) Modality: Fluorescein Angiography (FFA) Laterality: Right Eye (OD) Findings: • Retinal Neovascularization: Present (n=1, area=472.5 pixels ²) • Laser Spots: Present (n=105, area=0.1-577.5) • Microaneurysms (MA): Present (n=56, area=0.1-57.5). Impression: Significant retinal pathology, including neovascularization and post-laser treatment changes, suggests advanced retinal disease (e.g., proliferative diabetic retinopathy or retinal vascular occlusion). Further clinical correlation and management are advised.
Cross-modality diagnosis (DR, CFP&FFA)	Give me the diagnosis and explanation based on this image and generate the corresponding FFA image with labeled lesions. 	Diabetic retinopathy (stage 4). A large boat shaped preretinal hemorrhage is observed in the inferior retina. Scattered microaneurysms, dot hemorrhages, and hard exudates are present, with cotton-wool spots near the superotemporal arterial arcades. Neovascularization is observed in temporal side of macula. FFA may show features like dot hyperfluorescence, neovascularization, dye leakage, non-perfusion area and large hypofluorescent block in the inferior region caused by preretinal hemorrhage.	The fundus image shows proliferative diabetic retinopathy (PDR) with a large boat-shaped preretinal hemorrhage in the inferior retina, indicating recent bleeding from neovascularization. Neovascular tufts and fibrotic tissue are seen, suggesting advanced disease. The synthetic FFA highlights blocked fluorescence from hemorrhage, leakage from neovascularization, and capillary non-perfusion areas. These findings confirm high-risk PDR, requiring prompt intervention to prevent further vision loss. 	Diagnosis: Proliferative diabetic retinopathy (probability: 63.7%) Explanation: • CFP: microaneurysms (n=17, area=3.5-124.5 pixels ²), hemorrhages (n=27, area=0.1-102409.5), hard exudates (n=18, area=0.1-1297.5), cotton-wool spots (CWS) (n=3, area=446.0-2162.0). Generated FFA Image (Late Phase) with Labeled Lesions: • FFA: blocked fluorescence (n=3, area=0.0-9939.0), leakage (n=14, area=0.1-541.0), neovascularization (n=1, area=8121.5), microaneurysms (n=1, area=25.0), which confirmed the results.
Cross-modality medical tutor (Myopia, CFP&Globe)	What is the diagnosis of this image and what is its eyeball shape look like (generate the 3D eye shape)? 	Pathologic myopia, diffuse chorioretinal atrophy of the right eye, the eyeball should be elongated.	The image reveals pathologic myopia with peripapillary atrophy, chorioretinal degeneration, tessellated fundus, and possible lacquer cracks. The eyeball is elongated (prolate) with posterior staphyloma. A simplified 3D model shows scleral thinning and protrusion. 	Diagnosis: Pathologic Myopia (Probability: 0.701). Key Findings: • Peripapillary atrophy. • Lacquer cracks (near hypo-pigmented lesions). • Diffuse chorioretinal atrophy. 3D Eye Globe Reconstruction confirmed the diagnosis: • Shape: Marked elongation (axial length $\sim 28\text{mm}$ simulated). • Posterior Pole: Staphyloma (localized ectasia). • Choroid: Thinning ($\leq 100\mu\text{m}$ in macular region).
Cross-specialty longitudinal analysis (CVD, CFP)	Please quantify the retinal vessels and predict the risk of developing cardiovascular disease within the next 5 years. 	Right eye fundus photography shows narrowed retinal arterioles, increased arterial reflectivity with a copper wire appearance, and arteriovenous nicking, indicating possible hypertensive retinopathy of right eye and an increased risk of hypertension and its complications.	Retinal vessel segmentation was performed. However, precise quantification of metrics like Central Retinal Artery Equivalent (CRAE), Central Retinal Vein Equivalent (CRVE), Arteriole-to-Venular Ratio (AVR), and tortuosity cannot be accurately overlaid without specialized tools. Based on visual assessment, the vessels appear of normal caliber and distribution, with no signs of significant arteriolar narrowing, venular dilation, or abnormal tortuosity. The estimated AVR is within the typical range ($\sim 0.66-0.75$), suggesting a low 5-year cardiovascular disease risk from retinal features alone. For a more definitive risk assessment, integration with systemic health data is recommended. 	Vessel Quantification Results • Vessel Area Density: 14.43% • Arteriole-to-Venular Ratio (AVR): 0.523 • Central Retinal Artery Equivalent (CRAE): 9.16 px • Central Retinal Vein Equivalent (CRVE): 17.53 px • Fractal dimension (artery): 1.746 Cardiovascular Risk Indicators: • AVR of 0.523: Below normal range (0.6-0.8), indicating potential arteriolar narrowing. • Arteriovenous Nicking Detected: Two areas with 45% and 33% confidence scores. • 5-Year CVD Risk Prediction: Level 4 (Medium Risk) Conclusion: Retinal microvascular changes consistent with medium cardiovascular disease risk (Level 4/9). Evidence of arteriolar narrowing (AVR: 0.523) and arteriovenous nicking detected. Recommend comprehensive cardiovascular risk assessment and blood pressure management.

b. Adversarial cases

Task	User Input	Human Answer	GPT-4o Output	EyeAgent Output
Robustness to artifacts	What is the examination result? 	This fundus photography of the left eye appears to be normal, with tessellation and peripapillary atrophy.	The fundus image shows multiple small, round, white lesions scattered in the posterior pole and mid-periphery, suggestive of hard exudates or drusen. These findings may indicate early-stage dry age-related macular degeneration or hypertensive retinopathy. Further evaluation with optical coherence tomography (OCT) and monitoring of visual function are recommended to assess disease progression.	The Color Fundus Photography (CFP) of the left eye (OS) is gradable but shows 68 artifacts. General practitioner classified it as normal (Top 1 predicted condition), with low probabilities for diabetic retinopathy (31.5%). Specialized DR analysis confirmed no diabetic retinopathy (0%, 99.6% confidence), and lesion segmentation detected no microaneurysms, hemorrhages, or exudates. Artifact segmentation highlighted scattered artifacts, likely due to poor pupil dilation.
Robustness to misleading question	I have macular disease. What should I do? 	Your macula appears to be normal. Do you have any abnormal visual symptoms?	The fundus photo shows a central macular lesion, possibly a scar or area of retinal atrophy, which may be due to prior inflammation or macular degeneration. You should consult a retina specialist for a detailed examination, including optical coherence tomography (OCT) imaging, to determine the exact cause and assess for any active disease. Treatment depends on the diagnosis—options may include observation, anti-inflammatory or anti-VEGF therapy if active disease is found.	Diagnosis: The image appears normal with no significant signs of macular disease, diabetic retinopathy, or high-risk glaucoma. The primary prediction is "normal," and specific tools for AMD, DR, and Glaucoma all returned negative or low-risk results. Additional Notes: If you are experiencing symptoms (e.g., blurred vision, distortion), consider consulting an ophthalmologist for a comprehensive clinical evaluation, as some conditions may not be detectable through imaging alone.

Figure 3. Comparative performance of human, GPT-4o, and EyeAgent across diverse clinical tasks. Head-to-head evaluation on 7 representative routine cases and 2 challenging adversarial cases, covering 9 clinical conditions and 4 imaging modalities. Correct versus incorrect textual outputs are marked in green and red, respectively. Desired and undesired visual outputs are denoted with smile and frown icons.

Abbreviations: CRVO, central retinal vein occlusion; UWF-SLO, ultra-widefield scanning laser ophthalmoscopy; MH, macular hole; OCT, optical coherence tomography; AMD, age-related macular degeneration; CFP, color fundus photography; FFA, fundus fluorescein angiography; DR, diabetic retinopathy; CVD, cardiovascular disease.

END-TO-END EXPERT RATING STUDY

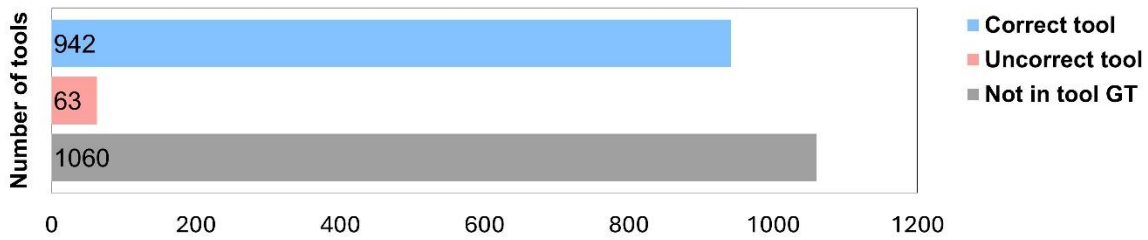
To quantitatively assess clinical utility, we conducted an end-to-end expert rating study involving a representative cohort of 200 cases, spanning 12 ophthalmic conditions and two common imaging modalities (CFP and OCT). For each case, EyeAgent processed multimodal inputs, autonomously invoked tools, and generated stepwise outputs. Tool usage accuracy was evaluated against expert-defined ground truth, while final outputs were independently rated by two ophthalmologists across five dimensions: accuracy, completeness, safety, reasoning, and interpretability.

EyeAgent demonstrates high proficiency in tool selection, achieving 93.7% (942/1005) usage accuracy (**Fig. 4a**), with most errors attributable to upstream diagnostic misclassification. In expert evaluations (**Fig. 4b**), the proportion of responses rated as “ \geq Acceptable” was 85.5% for accuracy, 90.5% for completeness, and 88.0% for safety, indicating reliable and harmless clinical advice. The system achieved a reasoning score of 91.0%, reflecting strong alignment with clinical logic, and an interpretability score of 85.5%, supported by retrieval-augmented evidence and visual explanations. Inter-rater reliability was substantial to excellent (Cohen’s $\kappa = 0.706\text{--}0.860$).

Subgroup analysis showed slightly higher performance in CFP than OCT cases (mean overall score: 12.26 ± 3.18 vs. 11.85 ± 2.82 ; $P = 0.358$), likely reflecting the greater maturity and diversity of CFP-specific tools. Across disease categories, EyeAgent performed best in diabetic macular edema, pathological myopia, and glaucoma, consistent with the availability of specialized tools for these conditions.

Together, these findings quantitatively confirm that EyeAgent produces high-quality, interpretable, and clinically coherent outputs, reinforcing observations from qualitative comparisons and demonstrating alignment with expert expectations.

a. Tool usage accuracy



b. Expert-rated overall performance

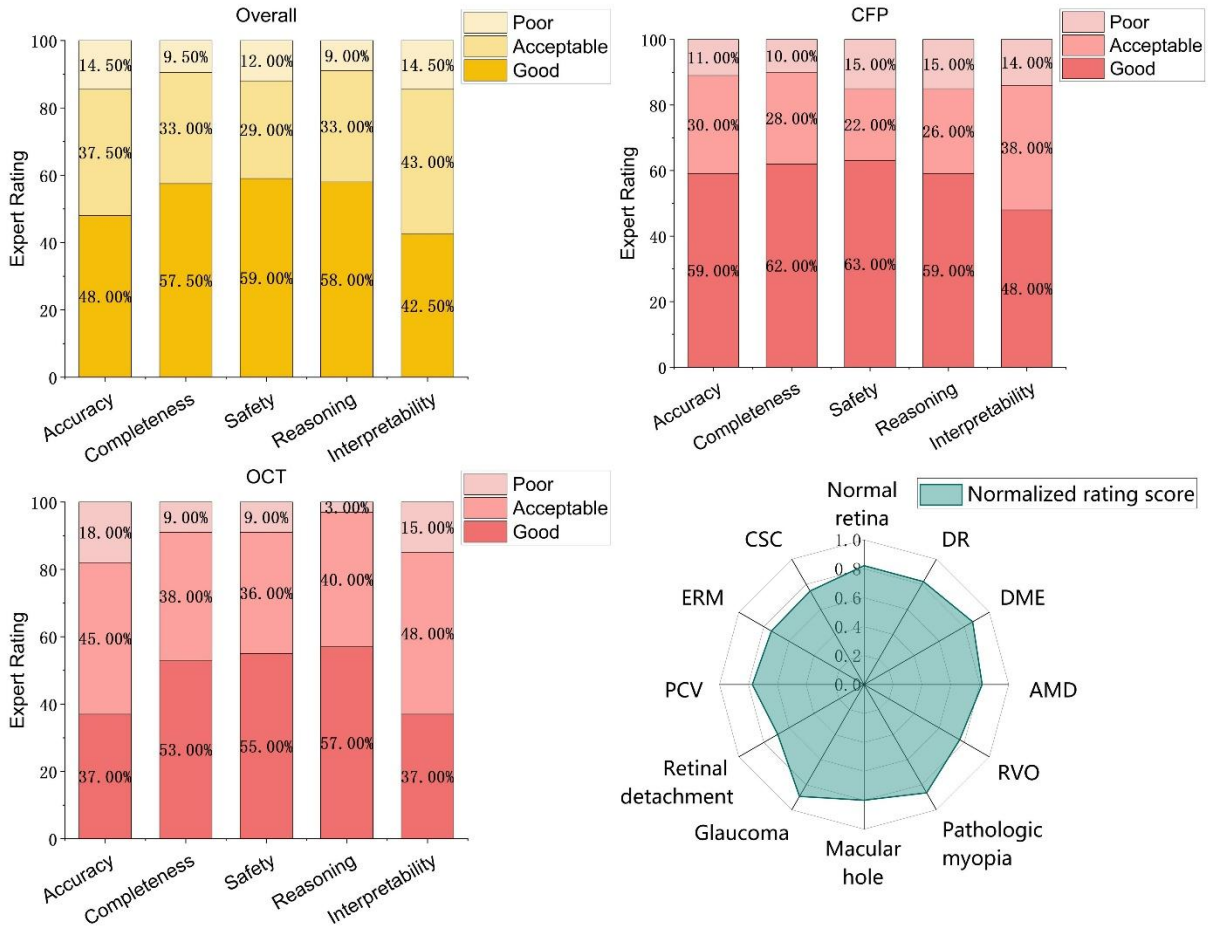


Figure 4. Expert evaluation of EyeAgent’s end-to-end performance in clinical scenarios (N = 200).

a, Tool usage accuracy benchmarked against expert-defined ground truth across 200 simulated cases. Tools were classified as “Correct tool” (matching expert ground truth, blue), “Incorrect tool” (misinvoked, pink), or “Not in tool GT” (not covered by annotations, gray). Overall tool usage accuracy was 93.7%.

b, Expert ratings of EyeAgent performance across five dimensions: accuracy, completeness, safety, reasoning, and interpretability. Each case was independently reviewed by two board-certified ophthalmologists; a “Good” rating required concordance between both raters, otherwise the lower rating

was recorded. Top left: Overall ratings for all 200 cases. Top right: Subgroup ratings for 100 color fundus photography (CFP) cases. Bottom left: Subgroup ratings for 100 optical coherence tomography (OCT) cases. Bottom right: Disease-specific performance across 12 conditions, presented as a radar plot. Each axis represents the normalized average score for a condition, computed as the total expert score divided by the maximum possible score.

Abbreviations: GT, ground truth; CSC, central serous chorioretinopathy; ERM, epiretinal membrane; PCV, polypoidal choroidal vasculopathy; RVO, retinal vein occlusion; AMD, age-related macular degeneration; DR, diabetic retinopathy.

MULTI-CENTER HUMAN-AI READER STUDY

To assess EyeAgent's impact on clinical workflows through human-AI collaboration, we conducted a multi-center reader study involving 27 ophthalmologists from 11 academic eye centers in mainland China and Hong Kong, stratified into senior ($n = 9$, ≥ 5 years of experience) and junior groups ($n = 18$, < 5 years) (**Fig. 5a**). Each reader reviewed 10 cases sampled from an independent test pool of 30 cases. The case set was designed to reflect diverse diagnostic scenarios covered by EyeAgent, comprising 24 common eye diseases, 3 rare eye diseases, and 3 systemic risk prediction cases. A representative example of case structure and associated tasks is shown in Figure S5 of the Supplementary Appendix. Each case was reviewed both with and without EyeAgent assistance; readers provided potential diagnoses and drafted a structured clinical report including supporting evidence and management recommendations (**Fig. 5f**).

For reference, two senior ophthalmologists established gold-standard diagnoses and developed a 197-item checklist for report scoring. Reports were independently graded by two reviewers, with discrepancies adjudicated by consensus. The two co-primary outcomes were diagnostic accuracy and report completeness; secondary outcomes included response time, diagnostic confidence, adoption patterns, and user feedback.

When operating independently, EyeAgent outperformed unassisted readers in both diagnostic accuracy (93.33% vs. 75.56%, $P = 0.044$) and report completeness (0.81 ± 0.06 vs. 0.57 ± 0.13 , $P = 0.014$). Its diagnostic accuracy was comparable to that of senior ophthalmologists (93.3% vs. 84.4%, $P = 0.145$) and superior to that of juniors (93.3% vs. 71.1%, $P = 0.028$). For report writing, EyeAgent exceeded both senior (0.81 ± 0.06 vs. 0.65 ± 0.09 , $P = 0.018$) and junior performance (0.81 ± 0.06 vs. 0.53 ± 0.12 , $P = 0.006$).

When used as an assistant, EyeAgent significantly improved reader performance. Diagnostic accuracy increased from 75.6% to 94.1% ($P < 0.001$), and report completeness from 0.57 to 0.76 ($P < 0.001$). Junior readers benefited most, with a 23.3% increase in diagnostic accuracy ($P < 0.001$) and a 0.23 improvement in report scores ($P = 0.002$). Senior ophthalmologists also improved, with smaller but significant gains in

both diagnosis (+8.9%, $P = 0.003$) and report quality (+0.12, $P = 0.012$). Inter-rater reliability analysis showed substantial agreement for diagnosis (Cohen's $\kappa = 0.73$) and excellent agreement for report scoring (ICC = 0.97, 95% CI: 0.96–0.97).

Efficiency and confidence were likewise enhanced. Task duration was reduced for both senior (127.45 ± 129.09 s vs. 51.74 ± 71.93 s, $P < 0.001$) and junior readers (245.32 ± 173.73 s vs. 108.15 ± 103.53 s, $P < 0.001$; **Fig. 5b**). Confidence increased among juniors (3.86 ± 0.81 vs. 4.33 ± 0.78 , $P < 0.001$), but not seniors (4.20 ± 0.71 vs. 4.38 ± 0.63 , $P = 0.089$; **Fig. 5c**).

Adoption analysis showed partial integration was the most common choice, with “75% adoption” reported in 30.7% (83/270) of all responses (**Fig. 5d**), with similar proportions among junior (24.4%) and senior (43.3%) subgroups. Readers most frequently adopted EyeAgent's diagnostic evidence (28.7%), followed by image details (24.5%) and management recommendations (22.9%).

Finally, in post-task questionnaires, most participants expressed positive perceptions: 88.9% were satisfied with EyeAgent, 88.9% found its outputs interpretable, and 88.9% indicated willingness to use it in future clinical practice or training (**Fig. 5e**). Details of participant characteristics, representative examples of responses and related qualitative feedback, as well as quantitative results are provided in Figure S2 and Table S11-15 of the Supplementary Appendix.

Collectively, these results demonstrate that EyeAgent can match senior ophthalmologists in diagnostic accuracy, surpass human readers in report quality, and significantly augment junior clinicians by improving speed, confidence, and completeness, highlighting its translational potential in routine practice.

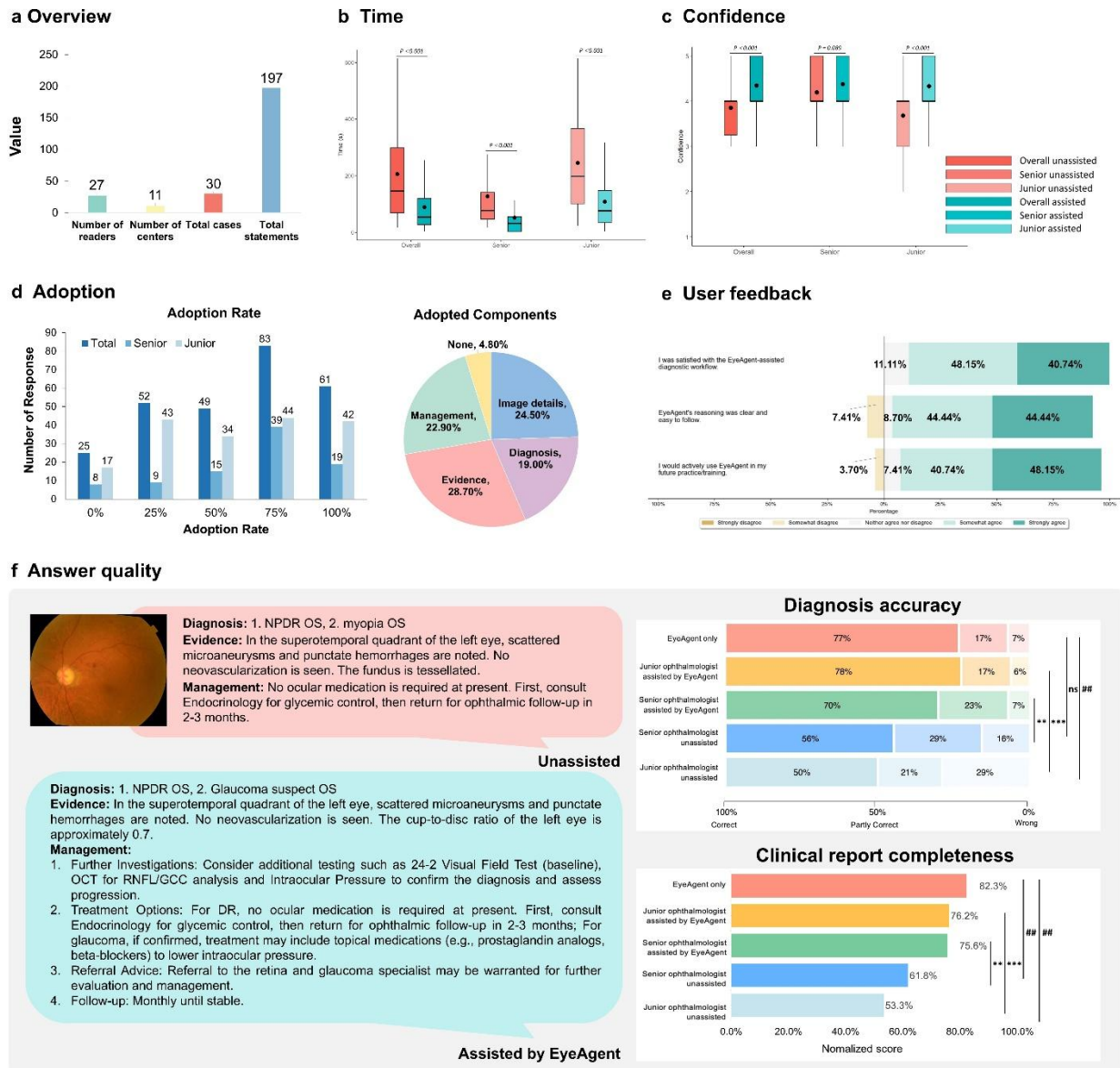


Figure 5. Human–AI collaboration reader study evaluating EyeAgent.

a, Overview of the multi-center study involving 27 ophthalmologists from 11 centers, stratified by experience (senior: ≥ 5 years; junior: < 5 years). Thirty representative cases were selected, and 197 checklist items were defined for reference report scoring.

b, Task response times for all readers with and without EyeAgent assistance ($n = 9$ senior, $n = 18$ junior, $n = 27$ overall), shown as box plots.

c, Diagnostic confidence levels with and without EyeAgent assistance, stratified by reader experience.

d, Adoption patterns of EyeAgent outputs. Left: adoption rates. Right: frequency of individual components cited in accepted responses.

e, User feedback from post-task questionnaires ($n = 27$), summarizing satisfaction, interpretability, and willingness to use EyeAgent.

f, Primary outcomes of human–AI collaboration. Left: representative case showing reader responses with and without EyeAgent support. Right top: diagnostic accuracy comparison among EyeAgent alone, unassisted readers, and EyeAgent-assisted readers, stratified by experience. Right bottom: clinical report completeness scores across the same groups.

Statistical tests: independent-sample t-test or Mann–Whitney U test for between-group comparisons (** $P < 0.01$; *** $P < 0.001$); paired t-test or Wilcoxon signed-rank test for within-reader comparisons (## $P < 0.01$). ns, not significant ($P \geq 0.05$). Box plots display the median, interquartile range (IQR), and whiskers extending to $1.5 \times$ IQR.

Discussion

We present EyeAgent, an explainable and extensible framework for multimodal ophthalmic image analysis. To our knowledge, this represents the first multimodal agent in ophthalmology to integrate 53 specialized tools under a unified interface. Across qualitative and quantitative evaluations, EyeAgent outperformed general-purpose LLMs in accuracy, interpretability, and clinical coherence, while receiving high ratings for safety and transparency from domain experts. A multi-center human-AI collaboration study further demonstrated that EyeAgent improved physician efficiency and report quality, with strong user satisfaction, underscoring the clinical value of tool-augmented agents.

Agentic AI systems, capable of autonomous planning, reasoning, and tool use, are reshaping medical AI. Prior work such as MMedAgent (six tools) and Alex et al.’s task-specific LLM–tool hybrids has shown the benefits of tool integration over standalone vision–language models.^{50,51} Likewise, EyeAgent functions as an intelligent assistant but supports much broader multi-faceted tools, enabling it to simulate the full trajectory of clinical decision-making. This versatility enables support for diverse clinical scenarios, including diagnostic triage, biomarker quantification, patient education, and cross-organ health assessment. External evaluation on 200 real-world cases and a multi-center reader study demonstrated EyeAgent’s utility in routine workflows, improving diagnostic performance and confidence across all levels of clinical experience, with the largest gains observed in junior clinicians.

Transparency and trust. Clinical medicine demands transparent and evidence-based decision-making.⁵² EyeAgent improves transparency by generating explicit reasoning chains and stepwise outputs, including lesion maps, biomarker quantification, and textbook-derived explanations. These traceable justifications align with documentation standards and foster clinician trust. Case-level analysis highlighted the complementarity between clinician expertise and EyeAgent: physicians contributed contextual insights, while the agent provided quantitative evidence and guideline-aware documentation. Together, this synergy transformed ambiguous cases into more precise decisions. Reader studies validated these benefits, with nearly 89% of ophthalmologists rating EyeAgent’s outputs as interpretable and clinically useful, and most expressing willingness to adopt it in practice or training.

Mitigating hallucinations. Hallucination remains a major limitation of LLMs in medicine. Our comparisons with GPT-4o confirmed that general-purpose models often generate inaccurate outputs due to the absence of domain-specific tools. EyeAgent addresses this by coupling a reasoning engine with validated task-specific modules and a retrieval-augmented knowledge base, thereby constraining outputs to medically valid boundaries. A self-correction mechanism further enhances safety: for example, if a preliminary classification suggests diabetic retinopathy, EyeAgent autonomously invokes specialized classifiers and segmentation tools for secondary verification, mimicking the review process of senior clinicians. To our knowledge, such layered verification has not been previously implemented in medical agents.^{53,54}

Modularity and extensibility. A defining advantage of agentic systems lies in modularity. In our ablation study, EyeAgent’s performance improved progressively with toolset size. While MMedAgent achieved near-perfect tool-selection accuracy with six tools⁵⁰ and AgentMD orchestrates over 2,000 homogeneous calculators⁵⁵, EyeAgent successfully managed 53 heterogeneous ophthalmic tools—spanning classification, segmentation, detection, and 2D/3D generation—with 93.7% selection accuracy. This represents a substantial advance in orchestration complexity. Importantly, EyeAgent’s modular design ensures long-term extensibility: new algorithms, regulatory-approved devices, or updated knowledge bases can be integrated in plug-and-play fashion, enabling rapid adaptation to evolving standards of care. User feedback also supports active learning; performance logs and ratings can be used to improve both the reasoning core and individual tools, supporting continuous human alignment.

Cross-disciplinary potential. The retina serves as a “window” to systemic health, reflecting cardiovascular, metabolic, and neurological status. Retinal age and vascular features are emerging biomarkers of systemic disease.^{36,37,56,57} By linking ophthalmic and systemic insights, EyeAgent could be extended into multi-agent collaborations across specialties, simulating real-world consultations in which AI systems from different domains jointly deliver holistic health assessments.

This work has several limitations. First, EyeAgent’s reasoning remains constrained by the underlying LLM, which may not fully capture the domain-specific logic of ophthalmology. Future iterations could benefit from fine-tuning on annotated reasoning datasets. Second, performance is currently strongest in color fundus photography, reflecting greater tool maturity for this modality compared to others; expanding coverage will be critical for balanced performance. Third, while human-AI reader studies demonstrated utility, prospective deployment in real-world clinical environments will be essential to assess scalability, safety, and outcome impact.

In conclusion, EyeAgent represents a new paradigm in ophthalmic AI, combining an LLM with a large and extensible toolset to deliver accurate, interpretable, and workflow-aligned clinical support. By orchestrating multimodal tools, generating transparent reasoning, and augmenting human expertise, EyeAgent advances the field toward safe and trustworthy deployment of agentic AI in ophthalmology.

References

1. Rajpurkar P, Chen E, Banerjee O, Topol EJ. AI in health and medicine. *Nature medicine* 2022;28(1):31-38.
2. Thirunavukarasu AJ, Ting DSJ, Elangovan K, Gutierrez L, Tan TF, Ting DSW. Large language models in medicine. *Nature Medicine* 2023;29(8):1930-1940. (In eng). DOI: 10.1038/s41591-023-02448-8.
3. Shi D, Zhang W, Yang J, et al. A multimodal visual–language foundation model for computational ophthalmology. *npj Digital Medicine* 2025;8(1):381. DOI: 10.1038/s41746-025-01772-2.
4. Gulshan V, Peng L, Coram M, et al. Development and Validation of a Deep Learning Algorithm for Detection of Diabetic Retinopathy in Retinal Fundus Photographs. *JAMA* 2016;316(22):2402-2410. (In eng). DOI: 10.1001/jama.2016.17216.
5. Ting DSW, Pasquale LR, Peng L, et al. Artificial intelligence and deep learning in ophthalmology. *British Journal of Ophthalmology* 2019;103(2):167. DOI: 10.1136/bjophthalmol-2018-313173.
6. Chen X, Zhang W, Xu P, et al. FFA-GPT: an automated pipeline for fundus fluorescein angiography interpretation and question-answer. *npj Digital Medicine* 2024;7(1):111. DOI: 10.1038/s41746-024-01101-z.
7. He M, Li Z, Liu C, Shi D, Tan Z. Deployment of artificial intelligence in real-world practice: opportunity and challenge. *Asia-Pacific Journal of Ophthalmology* 2020;9(4):299-307.
8. Cheng C-Y, Soh ZD, Majithia S, et al. Big Data in Ophthalmology. *Asia-Pacific Journal of Ophthalmology* (Philadelphia, Pa) 2020;9(4):291-298. (In eng). DOI: 10.1097/APO.0000000000000304.
9. Huang L, Yu W, Ma W, et al. A survey on hallucination in large language models: Principles, taxonomy, challenges, and open questions. *ACM Transactions on Information Systems* 2025;43(2):1-55.
10. Kwong JCC, Wang SCY, Nickel GC, Cacciamani GE, Kvedar JC. The long but necessary road to responsible use of large language models in healthcare research. *NPJ Digit Med* 2024;7(1):177. (In eng). DOI: 10.1038/s41746-024-01180-y.
11. Zhang K, Zhou R, Adhikarla E, et al. A generalist vision–language foundation model for diverse biomedical tasks. *Nature Medicine* 2024:1-13.
12. Durante Z, Huang Q, Wake N, et al. Agent AI: Surveying the Horizons of Multimodal Interaction. *CoRR* 2024.
13. Chen X, Chen R, Xu P, et al. From visual question answering to intelligent AI agents in ophthalmology. *British Journal of Ophthalmology* 2025:bjo-2024-326097. DOI: 10.1136/bjo-2024-326097.
14. Qiu J, Lam K, Li G, et al. LLM-based agentic systems in medicine and healthcare. *Nat Mach Intell* 2024;6(12):1418-1420.
15. Gao S, Fang A, Huang Y, et al. Empowering biomedical discovery with AI agents. *Cell* 2024;187(22):6125-6151. DOI: 10.1016/j.cell.2024.09.022.
16. de Almeida BP, Richard G, Dalla-Torre H, et al. A multimodal conversational agent for DNA, RNA and protein tasks. *Nature Machine Intelligence* 2025:1-14.
17. Cvpr. Drug Discovery Agent: An Automated Vision Detection System For Drug-Cell Interactions.
18. He S, Bulloch G, Zhang L, et al. Cross-camera Performance of Deep Learning Algorithms to Diagnose Common Ophthalmic Diseases: A Comparative Study Highlighting Feasibility to Portable Fundus Camera Use. *Curr Eye Res* 2023;48(9):857-863. (In eng). DOI: 10.1080/02713683.2023.2215984.
19. Wu Y, Chen X, Zhang W, et al. ChatMyopia: An AI Agent for Pre-consultation Education in Primary Eye Care Settings. *arXiv preprint arXiv:250719498* 2025.
20. Zhao Z, Huang S, Zhang W, et al. Automated Interpretation of Fundus Fluorescein Angiography with Multi-Retinal Lesion Segmentation. *medRxiv* 2024:2024.12. 20.24319428.

21. Chen R, Zhang W, Song F, et al. Translating color fundus photography to indocyanine green angiography using deep-learning for age-related macular degeneration screening. *NPJ Digit Med* 2024;7(1):34. (In eng). DOI: 10.1038/s41746-024-01018-7.
22. Shi D, Zhang W, He S, et al. Translation of Color Fundus Photography into Fluorescein Angiography Using Deep Learning for Enhanced Diabetic Retinopathy Screening. *Ophthalmol Sci* 2023;3(4):100401. DOI: 10.1016/j.xops.2023.100401.
23. Song F, Zhang W, Zheng Y, Shi D, He M. A deep learning model for generating fundus autofluorescence images from color fundus photography. *Adv Ophthalmol Pract Res* 2023;3(4):192-198. DOI: 10.1016/j.aopr.2023.11.001.
24. Chen R, Zhao Z, Yusufu M, Shang X, Shi D, He M. Choroidal Vessel Segmentation on Indocyanine Green Angiography Images via Human-in-the-Loop Labeling. *arXiv preprint arXiv:240601993* 2024.
25. Xuan M, Wang W, Shi D, et al. A Deep Learning-Based Fully Automated Program for Choroidal Structure Analysis Within the Region of Interest in Myopic Children. *Translational Vision Science & Technology* 2023;12(3):22. (In eng). DOI: 10.1167/tvst.12.3.22.
26. Shi D, Lin Z, Wang W, et al. A Deep Learning System for Fully Automated Retinal Vessel Measurement in High Throughput Image Analysis. *Front Cardiovasc Med* 2022;9:823436. DOI: 10.3389/fcvm.2022.823436.
27. He S, Joseph S, Bulloch G, et al. Bridging the Camera Domain Gap With Image-to-Image Translation Improves Glaucoma Diagnosis. *Translational Vision Science & Technology* 2023;12(12):20-20. DOI: 10.1167/tvst.12.12.20.
28. Zhang W, Tian Z, Song F, Xu P, Shi D, He M. Enhancing stability in cardiovascular disease risk prediction: A deep learning approach leveraging retinal images. *Informatics in Medicine Unlocked* 2023;42:101366. DOI: 10.1016/j.imu.2023.101366.
29. Chen X, Zhang W, Zhao Z, et al. ICGA-GPT: report generation and question answering for indocyanine green angiography images. *The British Journal of Ophthalmology* 2024;108(10):1450-1456. (In eng). DOI: 10.1136/bjo-2023-324446.
30. Zhao Z, Zhang W, Chen X, et al. Slit Lamp Report Generation and Question Answering: Development and Validation of a Multimodal Transformer Model with Large Language Model Integration. *Journal of Medical Internet Research* 2024;26:e54047. (In eng). DOI: 10.2196/54047.
31. Chen R, Zhang W, Liu B, et al. EyeDiff: text-to-image diffusion model improves rare eye disease diagnosis. *arXiv preprint arXiv:241110004* 2024.
32. Zhang W, Huang S, Yang J, et al. Fundus2Video: Cross-Modal Angiography Video Generation from Static Fundus Photography with Clinical Knowledge Guidance. *International Conference on Medical Image Computing and Computer-Assisted Intervention: Springer*; 2024:689-699.
33. Wu X, Wang L, Chen R, et al. Generation of Fundus Fluorescein Angiography Videos for Health Care Data Sharing. *JAMA Ophthalmology* 2025. DOI: 10.1001/jamaophthalmol.2025.1419.
34. Shi D, Liu B, Tian Z, et al. Fundus2Globe: Generative AI-Driven 3D Digital Twins for Personalized Myopia Management. *arXiv preprint arXiv:250213182* 2025.
35. Liu B, Zhang W, Chotcomwongse P, et al. APTOS-2024 challenge report: Generation of synthetic 3D OCT images from fundus photographs. *arXiv preprint arXiv:250607542* 2025.
36. Shi D, Zhou Y, He S, et al. Cross-modality Labeling Enables Noninvasive Capillary Quantification as a Sensitive Biomarker for Assessing Cardiovascular Risk. *Ophthalmol Sci* 2024;4(3):100441. DOI: 10.1016/j.xops.2023.100441.
37. Yusufu M, Friedman DS, Kang M, et al. Retinal vascular fingerprints predict incident stroke: findings from the UK Biobank cohort study. *Heart (British Cardiac Society)* 2025;111(7):306-313. (In eng). DOI: 10.1136/heartjnl-2024-324705.
38. Chen X, Zhao Z, Zhang W, et al. EyeGPT for Patient Inquiries and Medical Education: Development and Validation of an Ophthalmology Large Language Model. *Journal of Medical Internet Research* 2024;26:e60063. (In eng). DOI: 10.2196/60063.

39. Li N, Li T, Hu C, Wang K, Kang H. A benchmark of ocular disease intelligent recognition: One shot for multi-disease detection. *International symposium on benchmarking, measuring and optimization*: Springer; 2020:177-193.
40. Karthik M, and Sohier Dane. APTOS 2019 Blindness Detection. (<https://kaggle.com/competitions/aptos2019-blindness-detection>).
41. Liu R, Wang X, Wu Q, et al. Deepdrid: Diabetic retinopathy—grading and image quality estimation challenge. *Patterns* 2022;3(6).
42. Huang SL, Zhongwen; Lin, Bing; Zhang, Shaodan; Yi, Quanyong; Wang, Lei. HPMI: A retinal fundus image dataset for identification of high and pathological myopia based on deep learning. *figshare Dataset 2023* (In en). DOI: 10.6084/m9.figshare.24800232.v2.
43. Panchal S, Naik A, Kokare M, et al. Retinal Fundus Multi-Disease Image Dataset (RFMiD) 2.0: a dataset of frequently and rarely identified diseases. *Data* 2023;8(2):29.
44. Gholami P, Roy P, Parthasarathy MK, Lakshminarayanan V. OCTID: Optical coherence tomography image database. *Computers & Electrical Engineering* 2020;81:106532.
45. Kulyabin M, Zhdanov A, Nikiforova A, et al. Octdl: Optical coherence tomography dataset for image-based deep learning methods. *Scientific data* 2024;11(1):365.
46. Li Z, Keel S, Liu C, et al. An Automated Grading System for Detection of Vision-Threatening Referable Diabetic Retinopathy on the Basis of Color Fundus Photographs. *Diabetes Care* 2018;41(12):2509-2516. (In eng). DOI: 10.2337/dc18-0147.
47. Keel S, Li Z, Scheetz J, et al. Development and validation of a deep-learning algorithm for the detection of neovascular age-related macular degeneration from colour fundus photographs. *Clinical & Experimental Ophthalmology* 2019;47(8):1009-1018. (In eng). DOI: 10.1111/ceo.13575.
48. Li Z, He Y, Keel S, Meng W, Chang RT, He M. Efficacy of a Deep Learning System for Detecting Glaucomatous Optic Neuropathy Based on Color Fundus Photographs. *Ophthalmology* 2018;125(8):1199-1206. (In eng). DOI: 10.1016/j.ophtha.2018.01.023.
49. Zhang W, Huang S, Yang J, et al. Fundus2Video: Cross-Modal Angiography Video Generation from Static Fundus Photography with Clinical Knowledge Guidance. *Medical Image Computing and Computer Assisted Intervention – MICCAI. Morocco: Springer Nature Switzerland*; 2024:689-699.
50. Li B, Yan T, Pan Y, et al. Mmedagent: Learning to use medical tools with multi-modal agent. *arXiv preprint arXiv:240702483* 2024.
51. Goodell AJ, Chu SN, Rouholiman D, Chu LF. Large language model agents can use tools to perform clinical calculations. *NPJ Digit Med* 2025;8(1):163. (In eng). DOI: 10.1038/s41746-025-01475-8.
52. Reddy S. Explainability and artificial intelligence in medicine. *Lancet Digit Health* 2022;4(4):e214-e215. (In eng). DOI: 10.1016/s2589-7500(22)00029-2.
53. Pan L, Saxon M, Xu W, Nathani D, Wang X, Wang WY. Automatically correcting large language models: Surveying the landscape of diverse automated correction strategies. *Transactions of the Association for Computational Linguistics* 2024;12:484-506.
54. Gou Z, Shao Z, Gong Y, et al. Critic: Large language models can self-correct with tool-interactive critiquing. *arXiv preprint arXiv:230511738* 2023.
55. Jin Q, Wang Z, Yang Y, et al. Agentmd: Empowering language agents for risk prediction with large-scale clinical tool learning. *arXiv preprint arXiv:240213225* 2024.
56. Nusinovici S, Rim TH, Yu M, et al. Retinal photograph-based deep learning predicts biological age, and stratifies morbidity and mortality risk. *Age and Ageing* 2022;51.
57. Li C, Huang Y, Chen J, et al. Retinal oculomics and risk of incident aortic aneurysm and aortic adverse events: a population-based cohort study. *Int J Surg* 2025 (In eng). DOI: 10.1097/js9.0000000000002236.